JOURNAL OF THERMOPHYSICS AND HEAT TRANSFER
Vol. 9, No. 1, January–March 1995

Melting of a Cylindrical Polymeric Medium Subjected to Cyclic Torsional Shear Stress

William J. Mitchell* and I. S. Habib†
University of Michigan—Dearborn, Dearborn, Michigan 48128

The problem of phase change in a cylindrical polymeric material subjected to a constant amplitude cyclic torsional shear stress is analyzed. The steady state as well as the transient behavior of a long solid cylinder and a cylindrical shell are examined when the hysteresis heat generation G, in the medium is spacially variable and exponentially dependent on the local temperature in the form $G = \gamma f(r)\exp(A_r T)$. $f(r)$ accounts for the stress distribution within the solid, γ and A_r are related in part to the amplitude and frequency of the cyclic torque, and T is the sample local temperature. The analysis is carried through for heat generation parameters high enough to induce melting within the medium. The onset of melting and the propagation of the solid-liquid interface (two interfaces can arise), are examined for various heat generation parameters, external and internal boundary conditions for the case of a cylindrical shell. Analytical solutions for the steady-state temperature profiles are developed, and an explicit finite difference approach is used for the study of the full transient problem.

Nomenclature

A_r = parameter related to the effect of temperature on viscosity in a viscous heat-generating medium
Bi = biot number
Bi_1 = interior biot number
Bi_2 = exterior biot number
C_1, C_2 = constants of integration
c = specific heat capacity
h_1 = interior convective heat transfer coefficient
h_2 = exterior coefficient
k = thermal conductivity of solid
N_S = Stefan number
Q = limiting position of constant temperature region within solid (Fig. 1)
R = exterior radius of shell or cylinder
r = arbitrary radius in cylinder or shell
r_1 = interior radius of shell
S = position of first point to melt
S_1 = inner solid-liquid interface
S_2 = outer solid-liquid interface
T = temperature
T_L = melt temperature
T_∞ = ambient temperature
t = time
α = thermal diffusivity
β = dimensionless heat generation parameter
β_C = critical value of β
γ = rate of heat generation per unit volume
η_1 = dimensionless location of inner solid-liquid interface
η_2 = outer interface
λ = latent heat of fusion per unit volume
μ = exponent pertaining to the variation of shear stress with the radius r
ξ = dimensionless radius
ξ_1 = inner radius of shell
ϕ = dimensionless temperature
ϕ_S = exterior surf temperature
ϕ_0 = center temperature of solid cylinder
ϕ_1 = temperature of inner surface of shell
ρ = density
τ = dimensionless time
ω = dimensionless limiting position for region of constant temperature in the solid

Received Oct. 25, 1993; revision received April 13, 1994; accepted for publication May 19, 1994.
*Assistant Professor, Department of Mechanical Engineering.
†Professor, Department of Mechanical Engineering.

Introduction

IN our previous work on the subject of a polymeric material subjected to a cyclic but constant stress amplitude, we analyzed the thermal behavior of a solid undergoing 1) a cyclic axial stress with and without radiative heat transfer,[1,2] 2) a cyclic axial stress with phase change,[3] and 3) a cyclic bending stress with and without phase change in the medium.[4] In all of these previous cases, we have identified critical values for β, above which no thermal steady state prevails in the medium. Furthermore, for values of β above the critical values, the material exhibits a sharp rise in temperature up to the melting point and, ultimately, melting fronts are nucleated within the solid leading to a single solid-liquid interface for the case of an axial cyclic stress, although two interfaces can result for the case of a cyclic bending. We have also stated in this previous work the reasoning behind the inability of the medium to achieve a steady state. Briefly stated here, we indicate that metals can reach a steady-state thermal behavior under either a constant stress or a constant strain amplitude loading due to their high thermal diffusivities. Polymeric materials undergoing a cyclic stress with a constant stress amplitude do not reach a steady state if β exceeds certain values.[5–7] The hysteresis effects in such modes of loading result in a volumetric heat generation within the solid that is exponentially dependent on the local temperature. The fracture process of polymer and composite materials when subjected to cyclic loads, reveals certain features imprinted by this type of loading. It is very well known that high vibrational loads may lead to what is referred to as a thermal explosion or thermal rupture of these materials. We like to stress here that the present work is significantly important to the mechanical designers, because adequate knowledge about the fatigue behaviors of substances is crucial when that substance is exposed to high frequencies of cyclic loading. Related applications to the present work are in the areas of vibration tests of solid propellant, potential use of polymers in rotating machinery, high-frequency exposure of polymeric materials in space applications, fluid flow with nonlinear viscous dissipation, and

chemical reactions in vessels with Arrhenius form of heat release.[8-10]

In the present study, we explore the effects of a cyclic torsional stress with a constant amplitude imposed on either a long solid polymeric cylinder or a long polymeric cylindrical shell. First we analyze the cases of steady-state behavior for both with no phase change. Subsequently, the cases in which melting is initiated are considered. The propagation speed and the locations of the solid-liquid interfaces are obtained as functions of the interior and exterior conditions on the cylinders and β, which in these cases has values higher than the critical values. The steady-state solutions are obtained analytically. For the transient mode with and without phase change, an explicit finite difference technique is employed in which the stability criterion was mapped so that the solution obtained remained within the bound of stability.

Analysis

Figure 1 represents the model we have chosen for this study. It represents a cylindrical polymeric medium that could take the form of a solid cylinder (Fig. 1a), or a cylindrical shell (Fig. 1b) of some thickness. The cylinder is exposed to a cyclic torsional stress induced by some external torque at both ends. The shear stress variation in the radial direction induces a

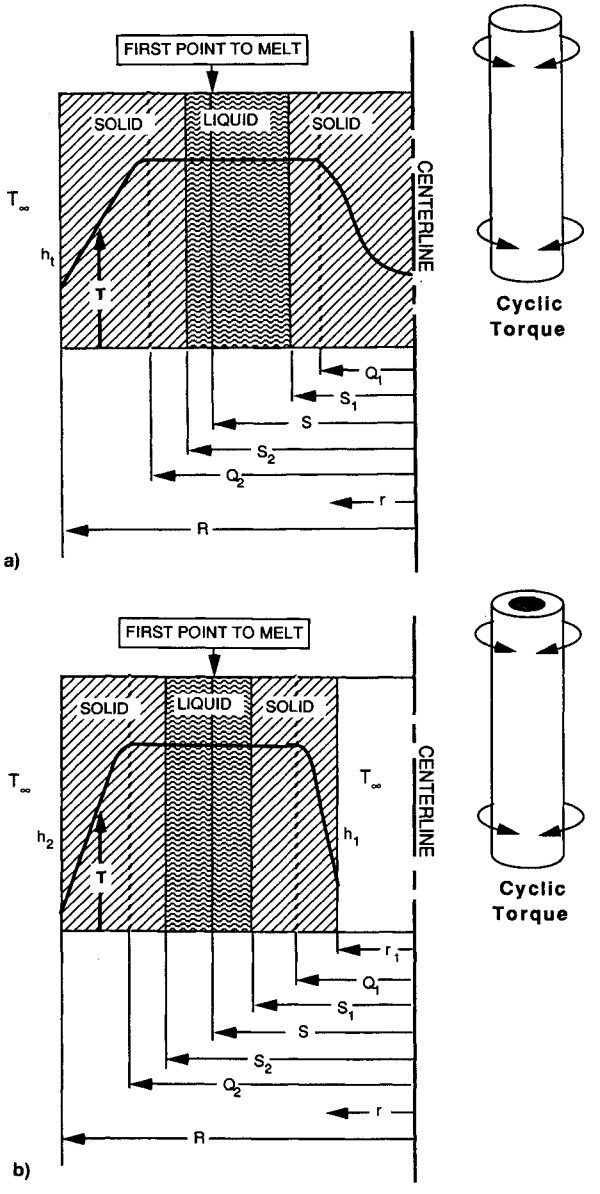

Fig. 1 Model chosen for study: a) solid cylinder and b) cylindrical shell.

radial variation in the energy generated, which is also exponentially dependent on the local temperature of the medium. The spacial variation of the energy generated is chosen to depend on the radius to some power. In one of our previous works,[4] which dealt with the medium undergoing bending stress, we have chosen that dependency to be quadratic. In the present work we choose that dependency to be more general so that the spatial variation of the energy depends upon the radius to a power μ. The physical properties of both the solid and liquid are considered equal and constant. A unique melt temperature T_L is assumed to exist, and when the liquid phase is formed, it is assumed to remain constantly at that temperature with the melting fronts being treated as cylindrical surfaces. Ahead of each solid-liquid interface, we consider that the heat generation maintains a solid region at the temperature of the melt T_L, bounded by Q_1 and S_1, and Q_2 and S_2 (see Fig. 1a). For the nucleation of a melt zone, the solid temperature just ahead of the nucleation site is expected to rise slightly above the melt temperature in order for the heat generation in that region to be transferred to the nucleation site and, hence, drive the front further into the solid. It is clear also that during fatigue loading of a material, a gradual failure should be expected that can cause changes in the form of the energy dissipation rate. Such an effect is not included in our analysis. Under the stated conditions, the energy equation representing the transient temperature distribution in the solid can be written in the form[1,4,5]

$$\rho c \frac{\partial T}{\partial t} = k\left(\frac{\partial^2 T}{\partial r^2} + \frac{1}{r}\frac{\partial T}{\partial r}\right) + \gamma\left(\frac{r}{R}\right)^{\mu} e^{A_1 T} \tag{1}$$

For the case of a solid cylinder, we consider that convection exists at the exterior surface so that

$$k\frac{\partial T}{\partial r} = h(T_\infty - T) \quad \text{at} \quad r = R \tag{2a}$$

$$\frac{\partial T}{\partial r} = 0 \quad \text{at} \quad r = 0 \tag{2b}$$

$$T = T_\infty \quad \text{at} \quad t = 0 \tag{2c}$$

For a cylindrical shell the boundary and initial conditions are

$$k\frac{\partial T}{\partial r} = h_2(T_\infty - T) \quad \text{at} \quad r = R \tag{3a}$$

$$-k\frac{\partial T}{\partial r} = h_1(T_\infty - T) \quad \text{at} \quad r = r_1 \tag{3b}$$

$$T = T_\infty \quad \text{at} \quad t = 0 \tag{3c}$$

In the presence of melting, the boundary conditions at the solid-liquid interfaces take the following forms:

$$\rho\lambda\frac{dS_1}{dt} = -\frac{1}{S_1}\int_{Q_1}^{S_1} r\left(\frac{r}{R}\right)^{\mu}\gamma e^{A_1 T}\,dr + \frac{1}{S_1}\left(kr\frac{\partial T}{\partial r}\right)_{r=Q_1} \tag{4a}$$

$$\rho\lambda\frac{dS_2}{dt} = -\frac{1}{S_2}\int_{Q_2}^{S_2} r\left(\frac{r}{R}\right)^{\mu}\gamma e^{A_1 T}\,dr + \frac{1}{S_2}\left(kr\frac{\partial T}{\partial r}\right)_{r=Q_2} \tag{4b}$$

$$T(S_1, t) = T(S_2, t) = T(Q_1, t) = T(Q_2, t) = T_L \tag{5}$$

The first terms on the right side of Eqs. (4a) and (4b) represent the heat generated within the proximity of the interfaces, and are responsible for propagating the interfaces further into the solid phase. In the absence of these terms, an interface can only be propagated by a surface temperature that exceeds the melting temperature of the medium. These boundary conditions at the interfaces are reduced to the more familiar form used in the literature when the heat generation is zero and

the liquid is kept at a constant temperature.[11-15] Let us introduce the following dimensionless variables:

$$\phi = A_r(T - T_\infty), \quad \xi = \frac{r}{R}, \quad \alpha = \frac{k}{\rho c}, \quad \tau = \frac{\alpha t}{R^2}$$

$$\beta = \frac{A_r \gamma R^2}{k} e^{A_r T_\infty}, \quad Bi_1 = \frac{Rh_1}{k}$$

$$Bi_2 = \frac{Rh_2}{k}, \quad N_S = \frac{c}{\lambda A_r}, \quad \eta_1 = \frac{S_1}{R}, \quad \eta_2 = \frac{S_2}{R}$$

$$\omega_1 = \frac{Q_1}{R}, \quad \omega_2 = \frac{Q_2}{R}, \quad \xi_1 = \frac{r_1}{R}$$

The energy equation and boundary conditions in terms of these variables become

$$\frac{\partial \phi}{\partial \tau} = \frac{\partial^2 \phi}{\partial \xi^2} + \frac{1}{\xi}\frac{\partial \phi}{\partial \xi} + \beta \xi^\mu e^\phi \tag{6}$$

For a solid cylinder we have

$$-\frac{\partial \phi}{\partial \xi} = Bi_2 \phi \quad \text{at} \quad \xi = 1 \tag{7a}$$

$$\frac{\partial \phi}{\partial \xi} = 0 \quad \text{at} \quad \xi = 0 \tag{7b}$$

$$\phi = 0 \quad \text{at} \quad \tau = 0 \tag{7c}$$

For a cylindrical shell we have

$$-\frac{\partial \phi}{\partial \xi} = Bi_2 \phi \quad \text{at} \quad \xi = 1 \tag{8a}$$

$$\frac{\partial \phi}{\partial \xi} = Bi_1 \phi \quad \text{at} \quad \xi = \xi_1 \tag{8b}$$

$$\phi = 0 \quad \text{at} \quad \tau = 0 \tag{8c}$$

The interface boundary conditions become

$$\frac{1}{N_S}\frac{d\eta_1}{d\tau} = -\frac{\beta}{\eta_1}\int_{\omega_1}^{\eta_1} \xi^{\mu+1} e^{\phi_L}\, d\xi + \frac{\omega_1}{\eta_1}\left[\frac{\partial \phi}{\partial \xi}\right]_{\xi=\omega_1} \tag{9}$$

$$\frac{1}{N_S}\frac{d\eta_2}{d\tau} = -\frac{\beta}{\eta_2}\int_{\omega_2}^{\eta_2} \xi^{\mu+1} e^{\phi_L}\, d\xi + \frac{\omega_2}{\eta_2}\left[\frac{\partial \phi}{\partial \xi}\right]_{\xi=\omega_2} \tag{10}$$

$$\phi(\eta_1, \tau) = \phi(\eta_2, \tau) = \phi(\omega_1, \tau) = \phi(\omega_2, \tau) = \phi_L \tag{11}$$

Steady-State Solution

We examine the steady-state behavior of the medium under the proposed nonlinear heat generation and the conditions under which a steady state can prevail. We examine the cases of a solid cylinder and a cylindrical shell. When a cylindrical shell is invoked, the boundary condition at the interior surface will be similar to that at an exterior surface, but with a different value of biot number *Bi*.

The energy equation becomes

$$\frac{d^2\phi}{d\xi^2} + \frac{1}{\xi}\frac{d\phi}{d\xi} + \beta \xi^\mu e^\phi = 0 \tag{12}$$

Let us introduce the following transformation variable in Eq. (12)[8]

$$e^Y = \xi^{\mu+2} e^\phi$$

so that Eq. (12) becomes

$$\xi^2 \frac{d^2Y}{d\xi^2} + \xi \frac{dY}{d\xi} + \beta e^Y = 0 \tag{13}$$

Multiplying Eq. (13) by $(dY/d\xi)\, d\xi$ and integrating yields

$$\int \left(\xi^2 \frac{d^2Y}{d\xi^2} + \xi \frac{dY}{d\xi}\right)\frac{dY}{d\xi}\, d\xi + \int \beta e^Y\, dY = \text{const} \equiv C_1 \tag{14}$$

or

$$\frac{1}{2}\left(\xi \frac{dY}{d\xi}\right)^2 + \beta e^Y = C_1 \tag{15}$$

Equation (15) is readily reduced to

$$\frac{d\xi}{\xi} = \frac{dY}{\sqrt{2(C_1 - \beta e^Y)}} \tag{16}$$

Equation (16) when integrated gives (for $C_1 \neq 0$)

$$Y = \text{ln}\left\{\frac{4C_1}{\beta}\frac{(C_2\xi)^{\sqrt{2C_1}}}{[1 + (C_2\xi)^{\sqrt{2C_1}}]^2}\right\} \tag{17}$$

and ϕ becomes

$$\phi = \text{ln}\left\{\frac{4C_1}{\beta}\frac{(C_2\xi)^{\sqrt{2C_1}}}{\xi^{2+\mu}[1 + (C_2\xi)^{\sqrt{2C_1}}]^2}\right\} \tag{18}$$

where C_1 and C_2 are yet to be determined.

Case of a Solid Cylinder

For ϕ to be finite at $\xi = 0$ (solid cylinder) we must have from Eq. (18)

$$\sqrt{2C_1} = 2 + \mu \tag{19}$$

and hence, ϕ takes the following form:

$$\phi = \text{ln}\left\{\frac{2(2+\mu)^2}{\beta}\frac{C_2^{2+\mu}}{[1 + (C_2\xi)^{2+\mu}]^2}\right\} \tag{20}$$

Evaluating Eq. (20) at the center $\xi = 0$, where $\phi = \phi_0$ yields the following expression for C_2:

$$C_2 = [\beta e^{\phi_0}/2(2+\mu)^2]^{1/(2+\mu)} \tag{21}$$

Accordingly, the expression for ϕ becomes

$$e^{\phi - \phi_0} = [1/(1 + \Omega\xi^{2+\mu})^2] \tag{22}$$

where

$$\Omega = [\beta e^{\phi_0}/2(2+\mu)^2] \tag{23}$$

The surface temperature ϕ_S is obtained from Eq. (22) by setting $\xi = 1$, which gives

$$e^{\phi_S - \phi_0} = [1/(1 + \Omega)^2] \tag{24}$$

In the limiting case of a prescribed surface temperature at $\xi = 1$, the value of the biot number becomes infinite, and $\phi_S = 0$. Equation (24) becomes

$$e^{\phi_0/2} = 1 + \Omega = 1 + [\beta e^{\phi_0}/2(2+\mu)^2] \tag{25}$$

For any biot number there is a critical value of β above which a steady state cannot be achieved. In the present case, where

the biot number becomes infinite, the β obtained will be the maximum critical value of β above which a steady state can never be achieved, we set $(d\beta/d\phi_0)$ from Eq. (25) to 0 and arrive at

$$\beta_{\text{maxcrit}} = [(2 + \mu)^2/2] = C_1 \tag{26}$$

For the case of a linear shear distribution (which yields a quadratic spatial variation in the hysteresis effects), the value of μ will be 2, and β takes the value of 8. This result is in agreement with our previous work.[2]

Returning to the general case, Eq. (24) relates the surface temperature ϕ_S and the center temperature ϕ_0 of a solid cylinder when β and μ are fixed. Since neither of these two temperatures is known, another relation is needed which is the surface convection. Hence, we have

$$\left(\frac{d\phi}{d\xi}\right)_{\xi=1} = -Bi_2\phi_S = -\frac{2(2 + \mu)\Omega}{1 + \Omega} \tag{27}$$

Now between Eqs. (24) and (27) we can obtain an implicit relation for ϕ_0 and, hence ϕ_S, and write

$$\phi_0 = 2 \ln(1 + \Omega) + \frac{2(2 + \mu)\Omega}{Bi_2(1 + \Omega)} \tag{28}$$

Equation (28) provides two additional important relations, one for $Bi_2 \to \infty$, and the other for $Bi_2 \to 0$. Recognizing that $(d\beta/d\phi_0) = 0$ gives $(d\Omega/d\phi_0) = \Omega$, Eq. (28) then yields at critical β

$$\Omega_{\text{crit}} = -[(2 + \mu)/Bi_2] + \sqrt{[(2 + \mu)/Bi_2]^2 + 1} \tag{29}$$

We can easily see from this relation that as $Bi_2 \to \infty$, $\Omega \to 1$. Using this limiting condition in Eq. (25) we arrive at the following important limiting value for ϕ_0 at maximum critical β for all values of μ

$$e^{\phi_0} = 4 \tag{30}$$

When $Bi_2 \to 0$, we have $\Omega \to 0$, $\phi_0 \to \phi_S \to 1$, and Eq. (28) gives another important relation relating β and Bi_2 for small values of Bi_2 in the form

$$\beta_{\text{CRITICAL}} = Bi_2[(2 + \mu)/e] \tag{31}$$

Case of a Cylindrical Shell

The general expression for ϕ is still given by Eq. (18). However, we have now the following two boundary conditions:

$$\frac{\partial\phi}{\partial\xi} = -Bi_2\phi_S \quad \text{at} \quad \xi = 1 \tag{32a}$$

$$\frac{\partial\phi}{\partial\xi} = Bi_1\phi_1 \quad \text{at} \quad \xi = \xi_1 \tag{32b}$$

Applying these conditions to Eq. (18) we obtain the following expressions relating C_1 and C_2 to ϕ_S and ϕ_1:

$$e^{\phi_S} = \frac{[2C_1 - (2 + \mu - Bi_2\phi_S)^2]}{2\beta} \tag{33}$$

$$e^{\phi_1} = \frac{[2C_1 - (2 + \mu + \xi_1 Bi_1\phi_1)^2]}{2\beta\xi_1^{2+\mu}} \tag{34}$$

$$\frac{\sqrt{2C_1}[1 - (C_2)^{\sqrt{2C_1}}]}{[1 + (C_2)^{\sqrt{2C_1}}]} = (2 + \mu - Bi_2\phi_S) \tag{35}$$

$$\frac{\sqrt{2C_1}[1 - (C_2\xi_1)^{\sqrt{2C_1}}]}{[1 + (C_2\xi_1)^{\sqrt{2C_1}}]} = (2 + \mu + \xi_1 Bi_1\phi_1) \tag{36}$$

Finite Difference Formulation for the Transient Case

The explicit finite difference form is employed in the solution of the transient problem. The corresponding finite difference forms of the equations become

for an exterior node

$$\phi_i^{\tau+1} = \phi_i^\tau - 2Bi_2\frac{\Delta\tau}{\Delta\xi[1 - (\Delta\xi/4)]}\phi_i^\tau + \frac{2\Delta\tau[1 - (\Delta\xi/2)]}{\Delta\xi^2[1 - (\Delta\xi/4)]}(\phi_{i-1}^\tau - \phi_i^\tau) + \beta\Delta\tau\xi^\mu \exp(\phi_i^\tau) \tag{37}$$

for an interior node

$$\phi_i^{\tau+1} = \phi_i^\tau + [\Delta\tau/(\Delta\xi)^2](\phi_{i+1}^\tau + \phi_{i-1}^\tau - 2\phi_i^\tau) + [\Delta\xi\Delta\tau/2\xi(\Delta\xi)^2][\phi_{i+1}^\tau - \phi_{i-1}^\tau] + \beta\Delta\tau\xi^\mu \exp(\phi_i^\tau) \tag{38}$$

for a center node

$$\phi_i^{\tau+1} = \phi_i^\tau + [4\Delta\tau/(\Delta\xi)^2][\phi_{i+1}^\tau - \phi_i^\tau] + \beta\Delta\tau\xi^\mu \exp(\phi_i^\tau) \tag{39}$$

for an interior surface node

$$\phi_i^{\tau+1} = \phi_i^\tau + \frac{2\Delta\tau}{(\Delta\xi)^2}\left[\frac{\xi_1 + (\Delta\xi/2)}{\xi_1 + (\Delta\xi/4)}\right][\phi_{i+1}^\tau - \phi_i^\tau] - \frac{2Bi_1\Delta\tau}{\Delta\xi[\xi_1 + (\Delta\xi/4)]}\xi_1\phi_i^\tau + \beta\Delta\tau\xi^\mu \exp(\phi_i^\tau) \tag{40}$$

The stability criterion was governed by the boundary nodes and must not be greater than the smallest $\Delta\tau$ resulting from the following two equations:

$$\Delta\tau_s = \frac{\Delta\xi^2(4 - \Delta\xi)}{4(2Bi_2\Delta\xi + 2 - \Delta\xi)} \tag{41}$$

$$\Delta\tau_1 = \frac{\Delta\xi^2(4\xi_1 + \Delta\xi)}{4(2Bi_1\xi_1\Delta\xi + 2\xi_1 + \Delta\xi)} \tag{42}$$

In all cases a $\Delta\tau$ smaller than that calculated above was used in the finite difference calculations. This produced a more closely spaced set of temperature distributions to select from for the temperature profile plots. Within the range used in this study, changes in $\Delta\tau$ had little effect on the temperature. For a set of conditions giving a very rapid temperature rise, at a peak temperature of 2.95, the change in ϕ was only 0.00012 when $\Delta\tau$ was changed from 0.000139 to 0.0000695.

The point of melt initiation changed from $\xi = 0.7524$ to 0.7522, and the final limits of the melt zone changed by less than 0.0001.

The regions between the outside surface and Q_2, and between the inside surface and Q_1, are solid regions in which the temperature increases from the surface to the melting point at the Qs, and so the energy Eq. (1) can be applied to both of these regions. Melting occurs because the temperature at Q_1 and at Q_2 reaches the melting point. From that point on, the boundary condition is that of a moving constant temperature boundary. The region between Q_1 and Q_2 is thereafter assumed to be at a constant temperature equal to the melting point. If a very low superheat is required to initiate melting, the liquid will be nucleated at various isolated points within this region and a "mush" will be produced. If a higher superheat is required, the heat will be transferred to the initial point of melting and that region will grow rather than forming multiple melt regions. We have assumed a single melt region

bounded by S_1 and S_2. As soon as melting is initiated, we separate the problem into two separate shells because there will be no heat transfer across the melt zone. Thus, the element in which melting is nucleated is split between the two shells. The heat generation within the region Q_1 to S_1, the movement of the boundary S_1, and the heat conduction out of Q_1 are described by the boundary condition (4a), and thus (4a) is the energy equation in the region from Q_1 to S_1. There is no heat generation in the liquid region and it is at a constant temperature, and so no additional energy equation is required to describe this region. In the finite difference program, this is handled by calculating the heat generated in the fully solid elements within Q_1 to S_1, adding the heat generated in the partially solid element at S_1, subtracting the heat conducted away at Q_1, and using the remainder to propagate the boundary S_1. The moving boundaries, Q_1 and Q_2 are located at the point of separation between solid, which is below the melting point and the solid that has reached the melting point. It is not necessary to track the exact partial element location of Q_1 and Q_2 during the finite difference program run, we just use the average temperature of the element. When the program terminates, Q_1 is equal to S_1, and Q_2 is equal to S_2. We then have two steady-state solid shells, the outermost one has an insulated inside surface at a radius of Q_2 at a temperature equal to the melting point. The inner shell has an insulated outer surface at Q_1, again, with the temperature equal to the melting point. In both cases the heat generation at Q is exactly equal to the heat conducted down the gradient, and thus steady state is attained. Since the liquid is at a constant temperature, there is no heat transfer through the liquid, and the thermophysical properties of the liquid other than the latent heat of fusion play no part in this analysis.

Results and Discussion

Figures 2–4 show the steady-state behavior of a solid cylinder exposed to a cyclic torque with no phase change. Figures 2 and 3 show the center and surface temperature of the solid as a function of β and for various values of biot number. The value of β at the rightmost position of each curve is β_C for the biot number indicated. It is clearly shown that β_C increases with an increase in the surface biot number. The stable solutions are those that fall on the lower branch of each curve, and any value of β greater than the critical value will not yield a thermally steady-state condition, but results in a continuously increasing temperature until that solid reaches the melting point. Figure 4 shows the surface temperature, center temperature, and β_C as a function of biot number. As biot number approaches infinity, the center temperature approaches the limiting value of $\frac{1}{2}$ (4), and β_C reaches the limiting value 8 (for $\mu = 2$), as predicted from Eqs. (25) and (26).

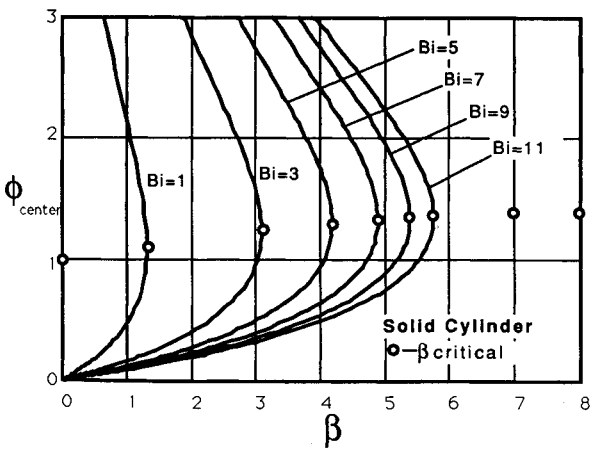

Fig. 2 Center temperature vs β for various values of biot number. β critical is indicated on each curve by an open ball (steady-state solid cylinder).

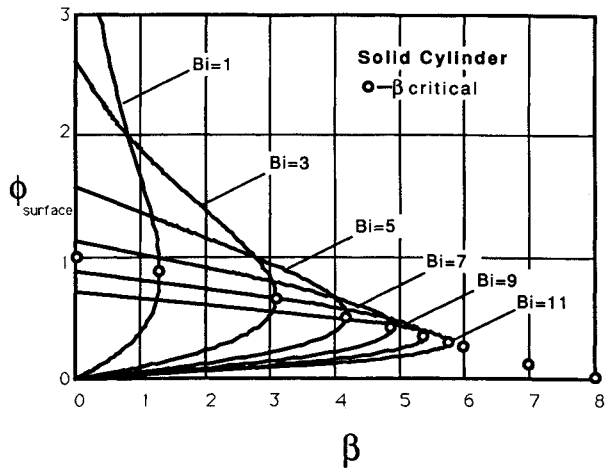

Fig. 3 Surface temperature vs β for various values of biot number. β critical is indicated on each curve by an open ball (steady-state solid cylinder).

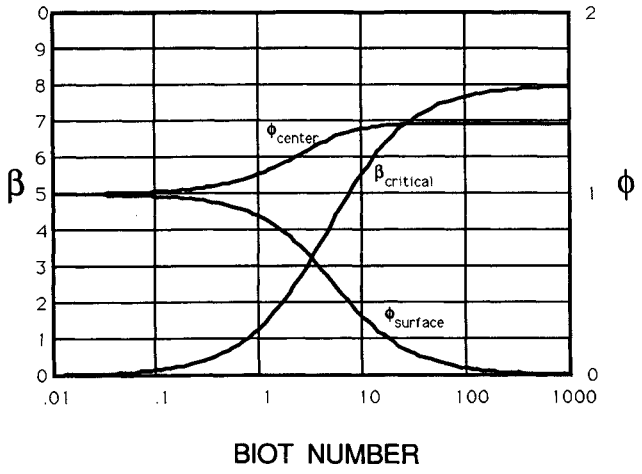

Fig. 4 Surface temperature, center temperature and critical values of β as a function of biot number (solid cylinder).

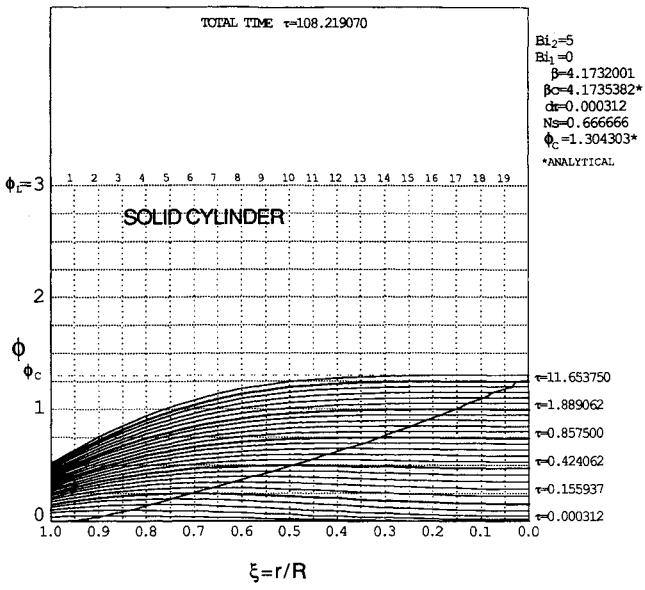

Fig. 5 Temperature profiles and locus of peak temperatures. (Solid cylinder, $Bi_2 = 5$, $Bi_1 = 0$, $\beta = 4.1732001$.)

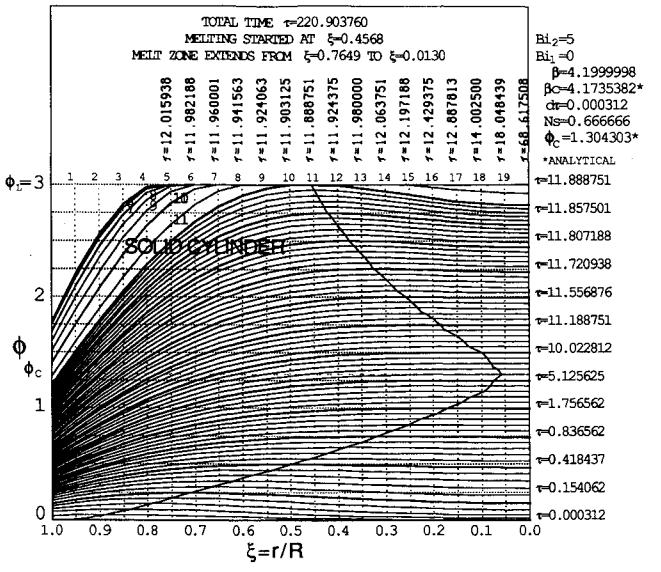

Fig. 6 Temperature profiles and locus of peak temperatures. (Solid cylinder, $Bi_2 = 5$, $Bi_1 = 0$, $\beta = 4.19999998$.)

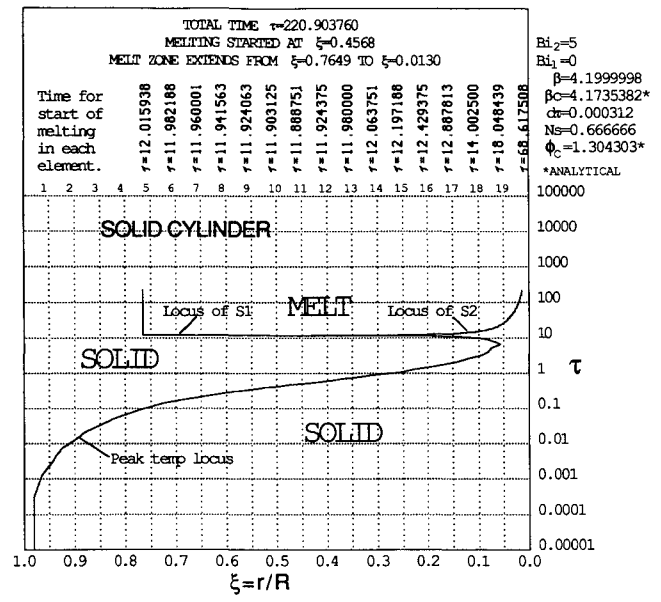

Fig. 7 Locus of peak temperatures and solid-liquid interfaces. Regions of solid and melt are labeled. (Solid cylinder, $Bi_2 = 5$, $Bi_1 = 0$, $\beta = 4.19999998$.)

Figure 5 shows a progression of the transient temperature distribution in a solid cylinder when β is slightly below the critical value β_C, and hence, no melting occurs. The uppermost curve represents the steady-state profile for the conditions indicated. The line moving diagonally across the figure is the locus of maximum temperature. The location of the maximum temperature was estimated by means of a quadratic interpolation using the temperatures of the elements adjacent to the maximum temperature element. The values of τ along the right boundary are referenced to this locus of maximum temperatures and the temperature locus (heavy line) passing through that maximum-temperature/τ combination. Note that the rate of temperature rise (indicated by the relative increments in τ) decreases rapidly as the critical temperature is approached. Note, particularly, the difference between $\tau = 11.653750$ at $\phi_{MAX} = 1.25$ and the total time $\tau = 108.219070$ at $\phi_C = 1.304303$. Figure 6 shows the thermal behavior of the same solid cylinder with β greater than the critical value. The location of the maximum temperature, as shown in this case, moves to the right until the critical temperature is reached, at which point the location of the maximum temperature re-

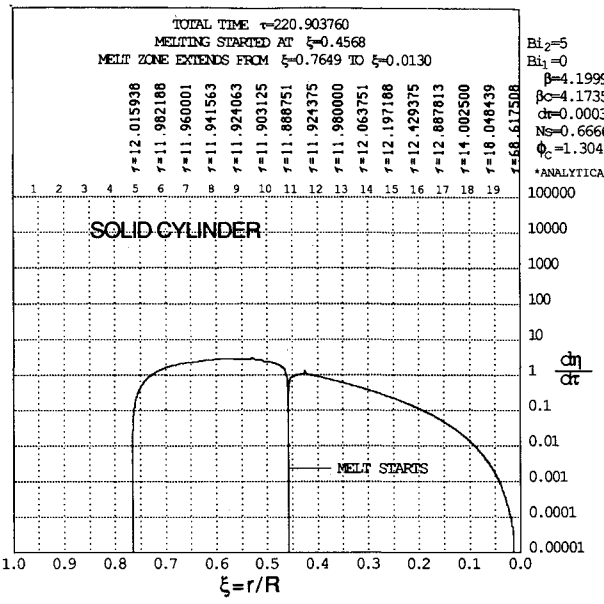

Fig. 8 Solid-liquid interface velocity. (Solid cylinder, $Bi_2 = 5$, $Bi_1 = 0$, $\beta = 4.19999998$.)

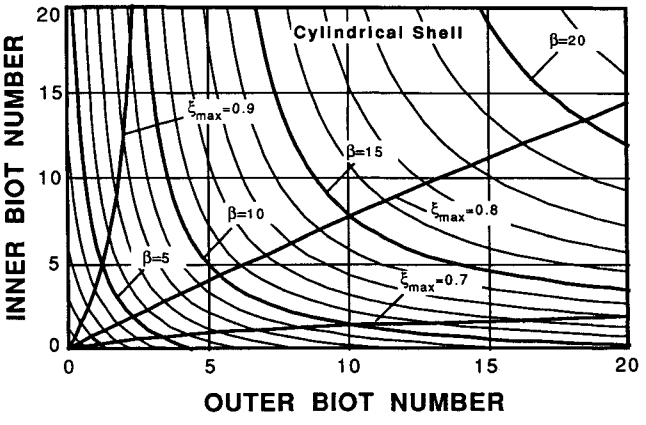

Fig. 9 Inner and outer biot numbers for various values of β. The location of the maximum temperatures, ξ_{max}, is also shown. The interior radius of the cylindrical shell is $\xi = 0.6$.

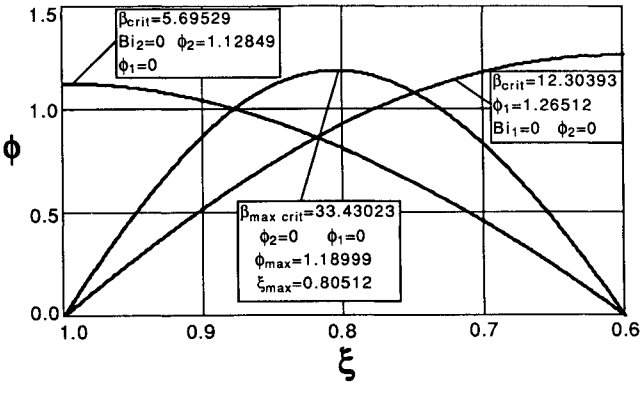

Fig. 10 Steady-state temperature distributions for a cylindrical shell with $\xi_1 = 0.6$ and various surface biot numbers.

verses direction and the temperatures continue to increase until the maximum value reaches the melting level. Subsequently, melting is initiated and two melting fronts are formed and start propagating in opposite directions. The interface moving towards the exterior surface stops at a location where the heat generation is balanced by the exterior convection to the ambient. The temperature profile shown at that time represents a steady-state profile in that portion of the solid. The interface moving towards the center continues to advance

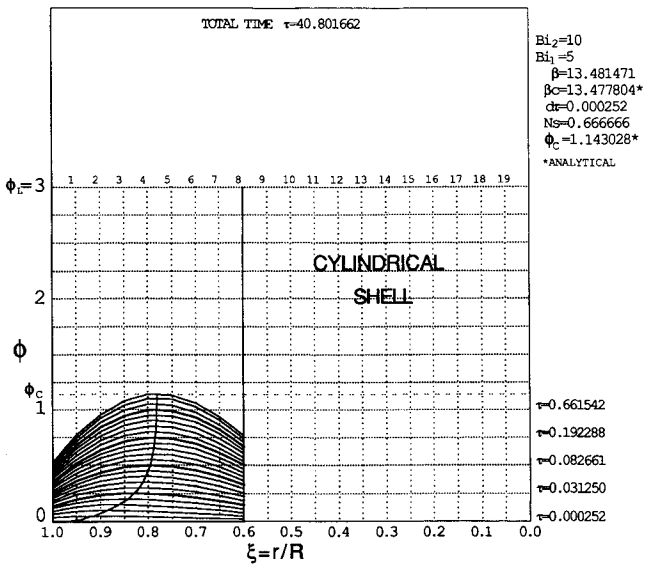

Fig. 11 Temperature profiles and locus of peak temperatures. (Cylindrical shell, $Bi_2 = 10$, $Bi_1 = 5$, $\beta = 13.481471$.)

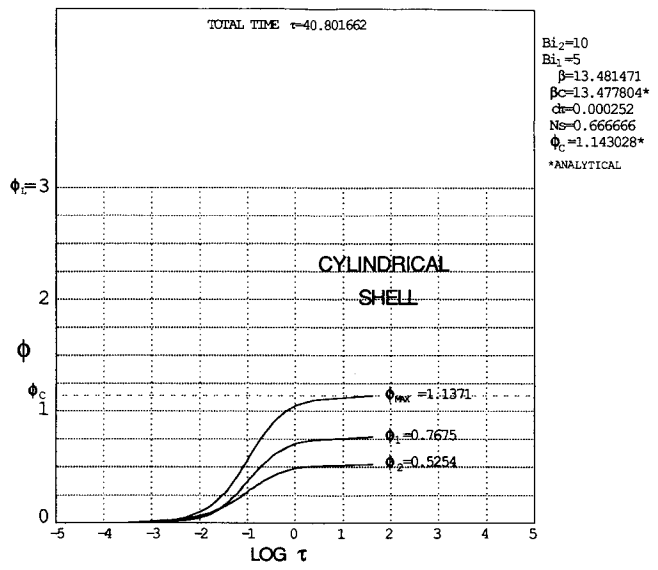

Fig. 12 Locus of peak and both surface temperatures. (Cylindrical shell, $Bi_2 = 10$, $Bi_1 = 5$, $\beta = 13.481471$.)

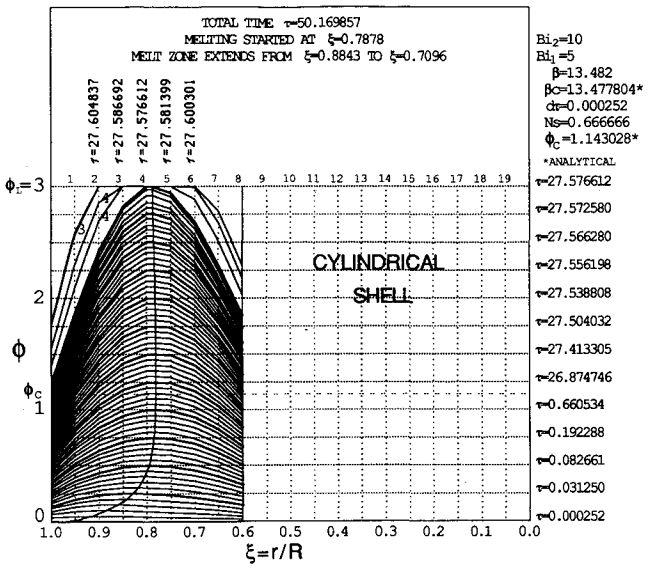

Fig. 13 Temperature profiles and locus of peak temperatures. (Cylindrical shell, $Bi_2 = 10$, $Bi_1 = 5$, $\beta = 13.482$.)

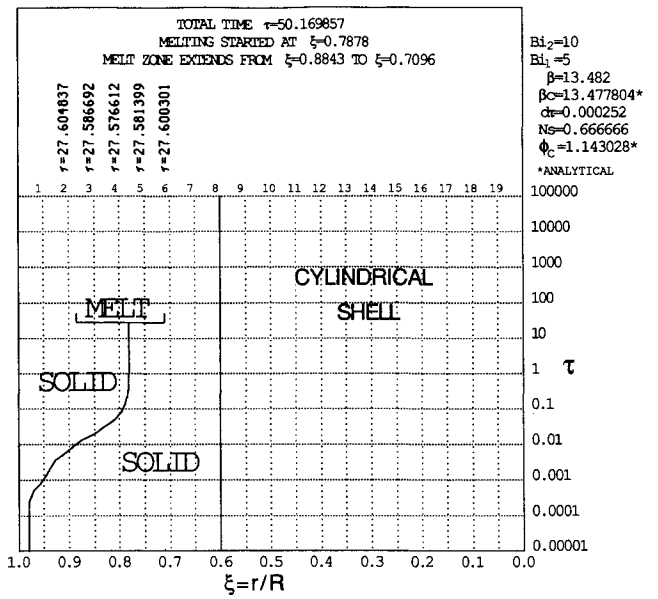

Fig. 14 Locus of peak temperatures and solid-liquid interfaces. (Cylindrical shell, $Bi_2 = 10$, $Bi_1 = 5$, $\beta = 13.482$.)

until the entire inner portion of the cylinder is melted. The finite difference elements are numbered across the top of the figure. The element number is located at the center of the corresponding element. The time when each element began to melt is shown above the element number. The boundaries of the elements lie between the numbers, and the time indicated is when the liquid interface reaches the element boundary. The first point to melt was at $\xi = 0.4568$ at $\tau = 11.888751$ in element 11. The liquid interface reached the left boundary of element 11 ($\xi = 0.475$) at $\tau = 11.903125$, and the right boundary was reached ($\xi = 0.425$) at $\tau = 11.924375$. The liquid interface reached the center element (element 20, $\xi = 0.025$) at $\tau = 68.71508$, and the limit of precision of the program was reached at $\tau = 220.903760$ when the liquid interface was at $\xi = 0.0130$. Steady state was realized on the left side when the liquid interface had reached $\xi = 0.7649$ in element 5. In Fig. 7 we show the width of the melt zone as a function of time for the same solid cylinder. Figure 8 shows the speed of the propagating fronts. Once melting is initiated, the two fronts approach their maximum speed very rapidly. Subsequently, the speeds decrease until their speeds become zero at the location where a steady state is reached in that portion of the solid and the interface stops advancing.

Mapping the solutions domain for the steady-state behavior of a cylindrical shell is far more complicated than that of a solid cylinder. Figure 9 shows a representative mapping of such a domain for a shell of inner radius $\xi_1 = 0.6$, and for various values of the inner and outer biot numbers. This figure identifies the values of β below which a thermal steady state can be achieved, and also shows the position ξ_{max} of the peak temperature in the solid. As can be expected, the figure shows the monotonic decrease in the value of β_C as the values of biot numbers on the exterior and the interior surfaces progressively decrease. Furthermore, the figure shows that insulating the exterior surface ($Bi_2 = 0$) has a more drastic effect on reducing the value of β_C than insulating the inner surface. For example, for an insulated exterior surface and a value of biot number at the inner surface of 12 ($Bi_1 = 12$), the value of β_C below which a steady state can be achieved is 4. However, if the inner surface is insulated and the outer biot number has a value of 12, the value of β_C is about 8.

Figure 10 shows a limiting behavior with no phase change in a shell having an inner radius of $\xi_1 = 0.6$. The figure shows the temperature profiles ϕ for three cases, namely 1) both surfaces at a prescribed temperature, $\phi_S = \phi_1 = 0$, curve A;

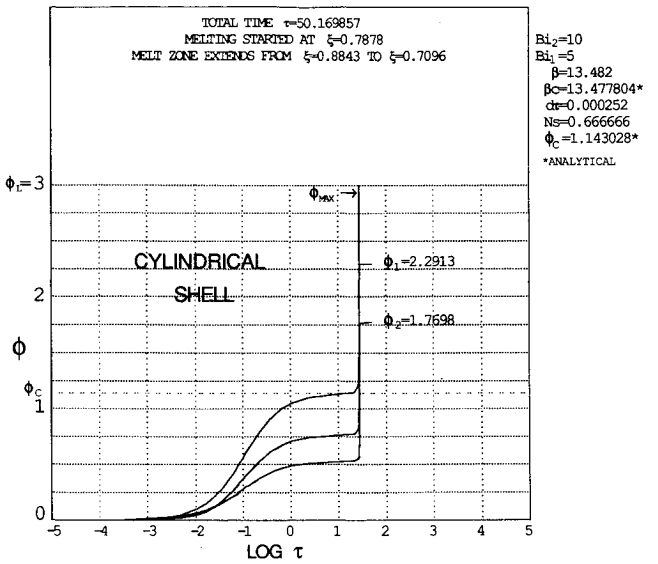

Fig. 15 Locus of peak and both surface temperatures. Inner and outer surface values are given at melt completion. (Cylindrical shell, $Bi_2 = 10$, $Bi_1 = 5$, $\beta = 13.482$.)

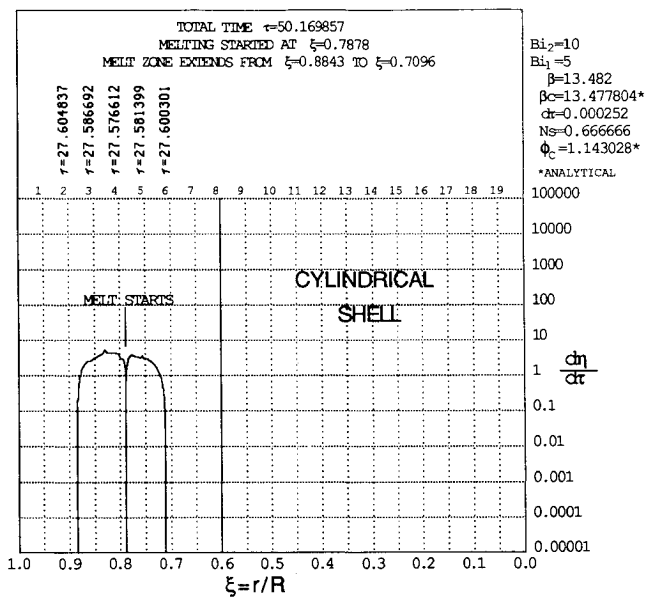

Fig. 16 Solid-liquid interface velocity. (Cylindrical shell, $Bi_2 = 10$, $Bi_1 = 5$, $\beta = 13.482$.)

2) the interior surface is insulated ($Bi_1 = 0$) while the exterior surface is at a prescribed temperature, $\phi_S = 0$, curve B; and 3) the exterior surface is insulated ($Bi_2 = 0$) while the interior surface is at a prescribed temperature, $\phi_1 = 0$, curve C. The curves are for different values of β because a single value of β will not yield a steady-state solution for all three cases. Here again, the figure shows that the case of a prescribed temperature on both surfaces exhibits a much higher tolerance to heat generation ($\beta = 33.43$), whereas for case 2, $\beta = 12.304$, and for case 3, $\beta = 5.695$.

Figures 11 and 12 show the transient temperature distribution in a shell and the loci of peak and both surface temperatures for $\beta < \beta_C$. The profiles show the progression to a steady state in a shell of inner radius of $\xi_1 = 0.6$. The peak temperature again shows an asymptotic approach to the critical temperature.

Figures 13–16 show the thermal behavior of a shell when $\beta > \beta_C$ and, hence, melting is initiated in the solid. In Fig. 13 the evolution of the transient profiles is shown until the temperature reaches the melting level. Here, also, two fronts are developed that then start moving radially in opposite di-

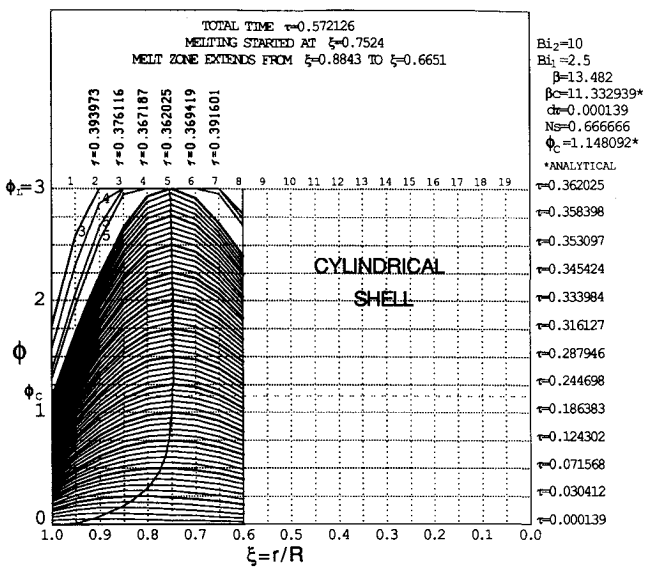

Fig. 17 Temperature profiles and locus of peak temperatures. (Cylindrical shell, $Bi_2 = 10$, $Bi_1 = 2.5$, $\beta = 13.482$.)

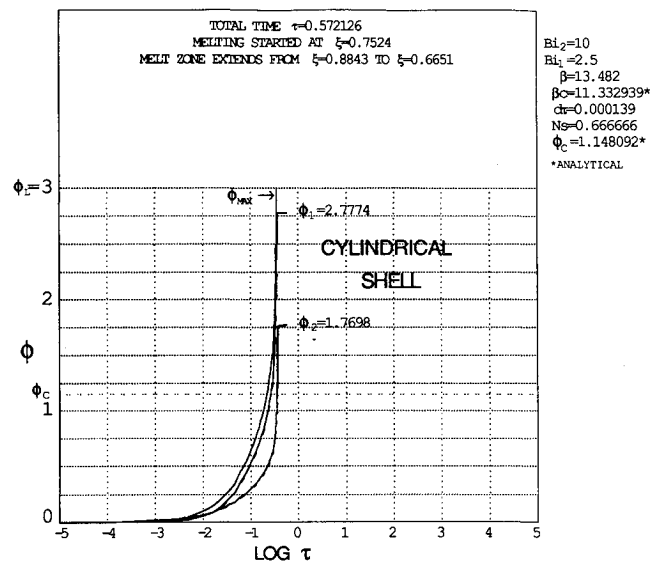

Fig. 18 Locus of peak and both surface temperatures. Inner and outer surface values are given at melt completion. (Cylindrical shell, $Bi_2 = 10$, $Bi_1 = 2.5$, $\beta = 13.482$.)

rections. The two fronts continue to advance until the heat generation on either side of the peak temperature is balanced by the respective convection to the ambient. Subsequently, two steady-state profiles are established, one close to the exterior surface and another close to the interior surface. Figure 14 shows the width of the melt zone in the shell, whereas Fig. 15 shows the loci of the peak and both surface temperatures. In Fig. 15 we show that when the liquid region has reached its maximum extent, the exterior and the interior surface temperatures reach the limiting values ($\phi_1 = 2.2913$ and $\phi_2 = 1.7698$), which are dictated by the values of biot numbers on each surface. The rate of rise of the peak temperature slows greatly as the critical temperature is approached, but as soon as the critical temperature is exceeded the temperatures rise very rapidly. Figure 16 shows the speeds of the propagating liquid fronts to be very similar to those of a solid cylinder. Here, the speeds of both fronts become zero at the locations where a steady state is reached in the exterior and the interior segments of the shell, where equality of heat generation and convection is established in both segments.

Figures 17 and 18 show the effect of decreasing the biot number on the interior surface while holding constant the

Table 1 Comparison of finite difference results with analytical computations

		Finite difference	Analytical	% Error
Figure 5	β_C	4.1732	4.1735	−0.0082%
Figure 11	β_C	13.481	13.478	+0.027%
Figure 12	ϕ_C	1.1371	1.1430	+0.521%
Figure 13	ω_2	0.8843	0.8824	+0.215%
Figure 14	ϕ_S	1.7698	1.7660	+0.215%

heat generation and the conditions on the exterior surface. Since β is well above the critical β, the temperatures rise very rapidly and show no retardation at the critical temperature. The point of initial melting moves toward the interior surface, compared to Fig. 13, because less heat is being extracted at that surface than in the preceding case. The steady-state condition on the exterior surface is identical to that realized in Fig. 13, $S_2 = 0.8843$ and $\phi = 3$ at the liquid interface, with $\phi_S = 1.7698$ and $Bi_2 = 10$ at the exterior surface with $\beta = 13.482$. Solving the set of simultaneous Eqs. (33–36) for the above conditions yields $\phi_S = 1.7660$ and $S_2 = 0.8824$, which is very close to the finite difference results. When melting begins, the solid divides into two concentric shells (or in the case of the solid cylinder, a cylinder and a shell), each having an insulated surface at a temperature equal to the melting temperature. Beyond this point there is no further thermal interaction between the two parts of the solid.

Accuracy of Results

Selected values taken from the figures are compared with the values obtained from analytical computations in Table 1.

The precision of the floating point package used in the finite difference runs was 8 digits with an error of ± 2 in the last place. Analytical calculations were made with 14-place accuracy.

Conclusions

The present work leads to the following conclusions:

1) Initiation of melting can appear in a solid cylinder or in a cylindrical shell when the solid is subjected to a cyclic torsional shear stress producing a β (the heat generation parameter) greater than β_C.

2) In a solid cylinder, for each surface biot number a critical β and ϕ_0 exist, above which melting will occur, but under no condition can a nonmelting steady state be realized if the center temperature reaches $\phi_0(4)$ or β exceeds $0.5(2 + \mu)^2$.

3) For the case of a cylindrical shell, the value of the biot number at the exterior surface has a more drastic effect on the thermal behavior and limits of heat generation than the inner value of biot number.

4) For the case of a cylindrical shell following the initiation of melting, two steady-state temperature profiles are reached in the solid, one towards the exterior surface and one towards the inner surface of the shell. The two solids are separated by the melt zone.

5) Once the melt zone has been created, the surface and inside solid zones no longer have any effect on each other, and the steady state at each surface is only determined by the value of β and the conditions prevailing at that one surface.

6) Mapping the various parameters that affect the behavior of a cylindrical shell is more complicated than for the solid cylinder.

7) Similar results were obtained for other values of Stefan number.

References

[1]Habib, I. S., "Radiative and Convective Effects on the Vibrational Heating of Semitransparent Polymers," *Journal of Spacecraft and Rockets*, Vol. 23, No. 1, 1986, pp. 124–126.

[2]Habib, I. S., "Radiative Effects on the Vibrational Heating of Polymers," *Journal of Spacecraft and Rockets*, Vol. 21, No. 5, 1984, pp. 496–501.

[3]Habib, I. S., "Melting of a Semitransparent Polymer Under Cyclic Constant Axial Stress," *Journal of Thermophysics and Heat Transfer*, Vol. 3, No. 3, 1989, pp. 355–358.

[4]Mitchell, W. J., and Habib, I. S., "Phase Change in a Polymeric Material Subjected to Cyclic Bending," *Heat Transfer in Phase Change*, American Society of Mechanical Engineers, ASME HTD, Vol. 205, 1992, pp. 27–36.

[5]Meinkoh, D., "Heat Explosion Theory and the Vibrational Heating of Polymers," *International Journal of Heat and Mass Transfer*, Vol. 24, No. 4, 1981, pp. 645–648.

[6]Schapery, R. A., "Thermomechanical Behavior of Viscoelastic Media with Variable Properties Subjected to Cyclic Loading," *Journal of Applied Mechanics*, Vol. 32, Sept. 1965, pp. 611–619.

[7]Schapery, R. A., "Effect of Cyclic Loading on the Temperature in Viscoelastic Media with Variable Properties," *AIAA Journal*, Vol. 2, No. 5, 1964, pp. 827–835.

[8]Herbert, D. M., "Thermal Explosion Theory for Reactants with Spatially Varying Surface Temperature," *Quarterly Journal of Mechanics and Applied Mathematics*, Vol. 41, Pt. 4, Oxford Univ. Press, Oxford, England, UK, 1988.

[9]Gray, P., and Lee, P. R., "Thermal Explosion Theory," *Oxidation and Combustion Reviews*, Vol. 2, 1967, pp. 1–183.

[10]Steggerda, J. J., "Thermal Stability: An Extension of Frank-Kamenetiski's Theory," *Journal of Chemical Physics*, Vol. 43, 1963, pp. 4446–4448.

[11]Hunter, L. W., and Kuttler, J. R., "The Enthalpy Method for Heat Conduction Problems with Moving Boundaries," *Journal of Heat Transfer*, Vol. 111, No. 2, 1989, pp. 239–242.

[12]Yao, L. S., and Prusa, J., "Melting and Freezing," *Advances in Heat Transfer*, Vol. 19, Academic Press, New York, 1989.

[13]Crank, J., "How to Deal with Moving Boundaries in Thermal Problems," *Numerical Methods in Heat Transfer*, edited by R. W. Lewis, K. Morgan, and O. C. Zienkiewicz, Wiley, New York, 1981.

[14]Lunardini, V. J., *Heat Transfer in Freezing and Thawing*, Elsevier, New York, 1991.

[15]Crank, J., *Free and Moving Boundary Problems*, Oxford Univ. Press (Clarendon), London, 1984.